

基于光纤可调滤波器的 1024 nm 锁模脉冲产生与放大研究

崔友硕, 张璐璐, 殷杰, 董自凯, 华玲玲, 田金荣, 宋晏蓉*

北京工业大学理学部, 北京 100124

摘要 1024 nm 波长的脉冲激光在角分辨光电子能谱测量等领域有着不可或缺的用处,因此采用基于非线性偏振旋转(NPR)锁模的全正色散掺镱光纤激光器作为种子源,搭建了包含光纤可调滤波器的主振荡功率放大系统,实现了 1024 nm 激光放大输出。理论上基于金斯伯格-朗道方程模拟了 NPR 锁模的耗散孤子脉冲演化过程,实验上获得了耗散孤子脉冲输出,并且研究了锁模脉冲的建立过程,将其与理论仿真结果相比,结果基本吻合。通过可调滤波器对种子光进行滤波,并进行预放大及放大实验,当放大级泵浦功率为 5 W 时,得到中心波长为 1024 nm、平均功率为 1.1 W、脉冲能量为 51 nJ、重复频率为 21.5 MHz、信噪比为 67.5 dB 的稳定锁模脉冲输出。

关键词 激光器; 光纤激光器; 锁模激光器; 激光放大器; 非线性偏振旋转; 耗散孤子

中图分类号 TN248

文献标志码 A

doi: 10.3788/CJL202148.0501019

1 引言

随着激光科学的发展,被动锁模光纤激光器被广泛应用于微加工^[1]、生物显微成像^[2]、光频梳和光谱学^[3]、国防和航天^[4]以及光纤通信^[5]等诸多领域。常见的被动锁模机制可以分为真实可饱和吸收体^[6-7]和人工可饱和吸收体^[8-10],但真实可饱和吸收体具有不易存放、损伤阈值低等缺点难以大规模商用化,此外非线性光学环形镜(NOLM)锁模激光器具有腔长较长、难以自启动、不易调节等缺陷。相比之下,非线性偏振旋转(NPR)锁模光纤激光器由于具有恢复时间短、损伤阈值高、易于调节的优点被广泛应用于超短脉冲的产生。

NPR 技术最早于 1992 年应用到掺铒光纤激光器中,实现了 1.55 ps 传统孤子脉冲输出^[11]。随后, Tamura 等^[12-13]通过调节腔内色散,先后获得了 77 fs 和 63 fs 的超短脉冲输出。2003 年, Buckley 等^[14]采用空间光结构,在空间光路中加入光栅对进行色散补偿,获得了 36 fs 的脉冲光输出。全正色

散(ANDi)NPR 锁模激光器也已经广泛应用于产生高功率和大能量的脉冲输出^[15]。此外, NPR 锁模光纤激光器还用于进行不同类型的孤子脉冲动力学研究,如耗散孤子(DS)^[16]、耗散孤子共振^[17]、类噪声^[18]、脉动孤子^[19]等。通过调整 NPR 结构中的波片和滤波片的角度可以调节锁模状态和波长,本实验采用了空间分离式结构的 NPR 锁模光纤激光器。

被动锁模光纤激光器振荡级的输出功率通常为毫瓦量级,难以满足实际应用,主振荡功率放大(MOPA)系统可以在有效保留种子光输出特性的基础上,对激光功率进行放大。1999 年, Zawischa 等^[20]报道了基于双包层掺铈离子光纤的 MOPA 放大系统,在 1064 nm 处得到了 5.5 W 的功率输出。2006 年, Ye 等^[21]搭建了基于双包层掺 Yb 光纤(YDF)的 MOPA 放大系统,获得了中心波长为 1064 nm,平均功率为 53.1 W 的超短脉冲输出。2014 年, Lin 等^[22]报道了采用波长可调的 NPR 锁模光纤激光器作为种子源的掺 Yb 光纤 MOPA 放

收稿日期: 2020-11-02; 修回日期: 2020-11-27; 录用日期: 2020-12-23

基金项目: 国家重点研发计划重点专项(2017YFB0405200)、国家自然科学基金(61975003)、北京市自然科学基金(4192015)

*E-mail: yrsong@bjut.edu.cn

大系统,通过两级预放大和两级主放大结构获得了平均功率 20 W 的激光输出。

角分辨光发射光谱 (ARPES) 可以通过动量分辨的方式直接获得电子的能带结构和电子的自能,是凝聚态物质电子结构研究中一种强大而独特的技术。对 1024 nm 激光多次倍频后可用作角分辨光电子能谱的光源,例如可用于稀土元素碲化物的电荷密度波能隙的测量等^[23]。Yb³⁺ 离子的发射峰主要在 1064 nm 附近,1024 nm 脉冲激光的获得相对较难,需要精细控制腔内滤波等参数,目前已有的 1024 nm 激光的报道主要集中在固体激光器^[24],而光纤激光器具有结构紧凑、成本低、稳定性好等优点,并可通过放大器弥补其功率低的缺点,具有很好的研究应用价值。

本文模拟了全正色散 NPR 锁模掺 Yb 光纤激光器中的脉冲动力学演化过程。实验上搭建了掺 Yb 光纤 MOPA 系统,种子源采用基于 NPR 锁模的掺

Yb 光纤激光器输出耗散孤子种子光脉冲,并且研究了锁模脉冲的建立过程。通过可调滤波器后可实现波长调节,先调至 1024 nm 处,对其进行预放大,再注入到主放大级中,放大后最大输出功率可达 1.1 W。

2 数值模拟

图 1 为用于数值模拟的全正色散 NPR 锁模光纤激光器理论模型。激光腔内增益介质为一段 30 cm 长的掺镱光纤,中心波长位于 1024 nm。三段单模光纤 (SMF1、SMF2、SMF3) 长度分别为 1、6、2 m,高斯型带通滤波器 (BPF) 的滤波带宽为 12 nm。利用偏振控制器 (PC) 进行偏振态调节,通过偏振分光棱镜 (PBS) 滤除脉冲能量较低的部分,采用 50% 输出比的输出耦合器 (OC) 进行输出。初始脉冲设置为一随机的高斯脉冲,光脉冲在腔中循环一圈后作为初始脉冲往复循环。激光在腔内的传输过程可由金斯伯格-朗道方程组进行描述。

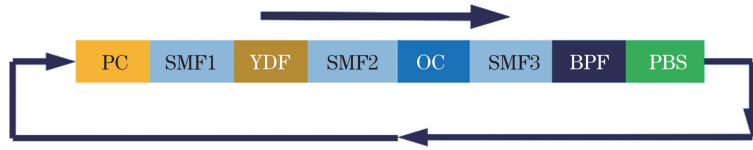


图 1 全正色散 NPR 锁模光纤激光器理论模型

Fig. 1 Theoretical model of ANDi NPR mode-locked fiber laser

$$\frac{\partial u}{\partial z} = -\frac{i\beta_2}{2} \frac{\partial^2 u}{\partial t^2} + i\gamma(|u|^2 + \frac{2}{3}|v|^2)u + \frac{i\gamma}{3} u^* v^2 \exp(-2i\Delta\beta z) + \frac{g}{2}u + \frac{g}{2\Omega_g^2} \frac{\partial^2 u}{\partial t^2} + (i\Delta\beta z)u, \quad (1)$$

$$\frac{\partial v}{\partial z} = -\frac{i\beta_2}{2} \frac{\partial^2 v}{\partial t^2} + i\gamma(|v|^2 + \frac{2}{3}|u|^2)v + \frac{i\gamma}{3} v^* u^2 \exp(2i\Delta\beta z) + \frac{g}{2}v + \frac{g}{2\Omega_g^2} \frac{\partial^2 v}{\partial t^2}, \quad (2)$$

式中: u 和 v 分别代表脉冲的两正交偏振分量的振幅; β_2 为光纤的群速度色散值 ($\beta_{2,YDF} = \beta_{2,SMF} = 20 \text{ ps}^2/\text{km}$); γ 为光纤的非线性系数 ($\gamma_{YDF} = \gamma_{SMF} = 4 \text{ W}^{-1} \cdot \text{km}^{-1}$); $\Delta\beta = 2\pi/L_b$, L_b 是双折射光纤的拍长; Ω_g 是增益带宽为 40 nm 的高斯形状的增益谱; g 为光纤的增益系数。考虑到增益饱和效应, g 可以写为

$$g = g_p \exp\left[-\frac{\int (|u|^2 + |v|^2) dt}{E_{\text{sat}}}\right], \quad (3)$$

式中: g_p 为小信号增益系数; E_{sat} 代表增益饱和能量, E_{sat} 的增加相当于泵浦强度的增加。在本文中, $g_{p,SMF} = 0$, $g_{p,YDF} = 18 \text{ m}^{-1}$, $E_{\text{sat}} = 200 \text{ pJ}$ 。

拟采用快速傅里叶变换法进行方程求解。通过适当调节两正交偏振态的强度比,当脉冲在腔内经

过多次往复循环后,可实现稳定的锁模脉冲输出,如图 2(a) 所示,随着腔内能量的积累,脉冲逐渐形成。图 2(b) 为光谱在腔内不同位置的演化形状,中心波长位于 1024 nm。可以看到激光通过 YDF 后光谱峰值显著提升,随后在 SMF2 中受非线性和色散效应的共同影响而形成典型的耗散孤子光谱,经过 OC 后强度衰减,脉冲继续在 SMF3 中传输,之后经过 BPF 滤波,通过 PBS 分束,再次循环。图 2(c) 为脉冲在腔内不同位置处的演化过程,通过 YDF 增益后,脉冲宽度和峰值显著增加,在 SMF2 中传输时受色散效应的影响脉冲能量逐渐向两沿分布,导致脉宽增加,峰值降低。随后由 OC 输出后腔内脉冲强度显著降低。图 2(d) 为腔内脉冲能量变化曲线,由于未考虑光纤损耗带来的影响,腔内脉冲能量基本为理想演化状态。

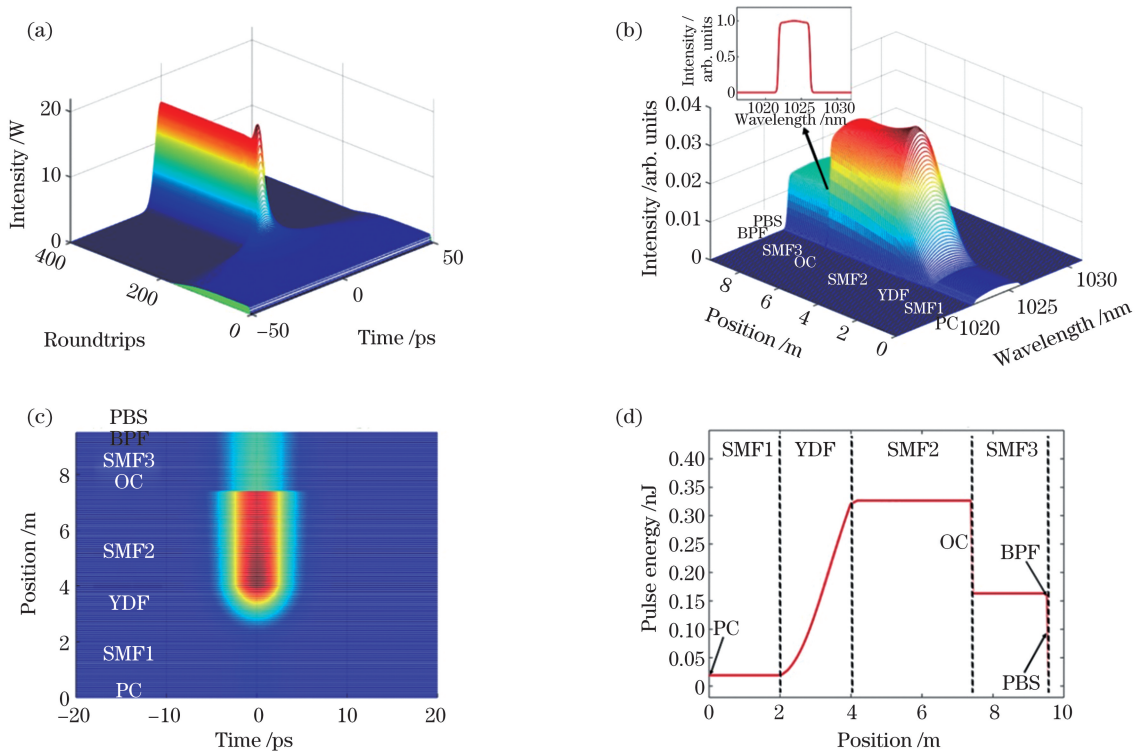


图 2 全正色散 NPR 锁模光纤激光器数值模拟结果。(a) 输出端脉冲演化;(b) 脉冲稳定时(第 400 圈时)腔内光谱演化;(c) 脉冲稳定时(第 400 圈时)腔内脉冲演化;(d) 第 400 圈时腔内脉冲能量演化图

Fig. 2 Numerical simulation results of ANDi NPR mode-locked fiber laser. (a) Evolution of output laser; (b) evolution of intra-cavity spectrum of stable state (at 400 roundtrip); (c) evolution of intra-cavity pulse of stable state (at 400 roundtrip); (d) evolution of intra-cavity pulse energy at 400 roundtrip

3 实验装置

图 3 为基于 NPR 锁模的 1024 nm 掺 Yb 光纤 MOPA 系统装置图,其中图 3(a)为种子源,图 3(b)为预放大级,图 3(c)为主放大级。种子源腔体采用环形腔结构,泵浦源为中心波长 976 nm、最高输出功率 650 mW 的模块化半导体激光器,腔内器件包括 980/1030 nm 波分复用器(WDM, Connet, 上海)、54 cm 长的掺 Yb 光纤(YDF, Yb1200-4/125, nLIGHT, 美国)、偏振无关隔离器(PI-ISO, Connet, 上海)、3 dB 输出耦合器、准直器(Col1、Col2, Connet, 上海);另外 1/4 波片、BPF(中心波长为 1030 nm, 滤波带宽为 12 nm)、PBS、1/2 波片、1/4 波片依次放置,用来调整腔内激光的偏振态以实现可饱和吸收效应。整个腔长约为 9.6 m,除增益光纤外腔内光纤均为普通单模光纤(SMF, 1060XP, Corning, 美国)。激光器腔内为全正色散,腔内净色散为 0.235 ps^2 。输出端连接了一个输出为 1% 的耦合器用于监测,另一端连接到光纤可调滤波器(TF, Connet, 上海)中,实现波长可调,以获

得不同参数的种子光。该滤波器可调滤波范围为 1020~1095 nm。预放大结构如图 3(b)所示,由中心波长为 976 nm、最大输出功率 300 mW 的泵浦源、980/1030 nm WDM 和一段 25 cm 长的 YDF (Yb1200-4/125, nLIGHT, 美国)组成,尾端由跳线头输出。放大级结构如图 3(c)所示,放大级前放置了一个隔离器(ISO),以防止背向光影响前级输出结果锁模特性。放大级采用中心波长为 976 nm、最大输出功率为 5 W 的多模半导体激光器泵浦,通过合束器将泵浦光耦合进大模场掺 Yb 增益光纤(LMA-YDF-10/130-VII, Nufern, 美国),经过准直隔离器(Col3, Connet, 上海)输出。脉冲测量系统由 6 GHz 示波器(DPO, 70604C, Tek, 美国)和 12.5 GHz 的光电探头(818-BB-35F, Newport, 美国)组成,光谱由光谱分析仪(AQ6370C, Yokogawa, 日本)探测,自相关仪(FR-103XL, FEMTOCHROME 公司, 美国)用来测量超短脉冲的自相关(AC)曲线,射频(RF)谱线采用射频谱仪(E4447A, Agilent, 美国)进行探测。

激光器种子光的形成是 NPR 机制,由波片、滤

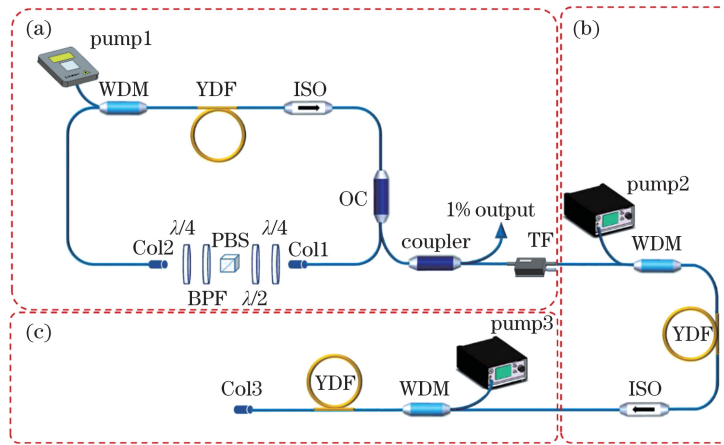


图 3 基于 NPR 锁模的 1024 nm 掺 Yb 光纤 MOPA 系统装置图。(a) 种子源;(b) 预放大级;(c) 主放大级
 Fig. 3 Schematic of 1024 nm Yb-doped fiber MOPA system based on NPR mode-locked. (a) Seed source laser; (b) pre-amplifier; (c) main amplifier

波片和 PBS 形成的人工可饱和吸收体实现。由于脉冲光中的高强度部分和低强度部分在光纤中受到的自相位调制(SPM)和交叉相位调制(XPM)等引起的非线性相移不同,导致它们的偏振方向有所差异,通过波片和 PBS 后,脉冲高强度部分被增益放大,脉冲低强度部分被损耗,经过多次往返,实现锁模输出。由于 NPR 属于快饱和吸收体锁模,所以更有利于超短脉冲的产生。

4 实验结果

在实验中,调节波片和 BPF 至适当角度,当泵浦功率为 355 mW 时,光纤激光器可实现耗散孤子脉冲输出。增加泵浦功率至 385 mW,激光器始终运转在耗散孤子状态,继续增加泵浦功率,脉冲由于能量过大而破裂,锁模状态消失。图 4 为振荡级输出特性曲线,其中图 4(a)为输出功率随泵浦功率变

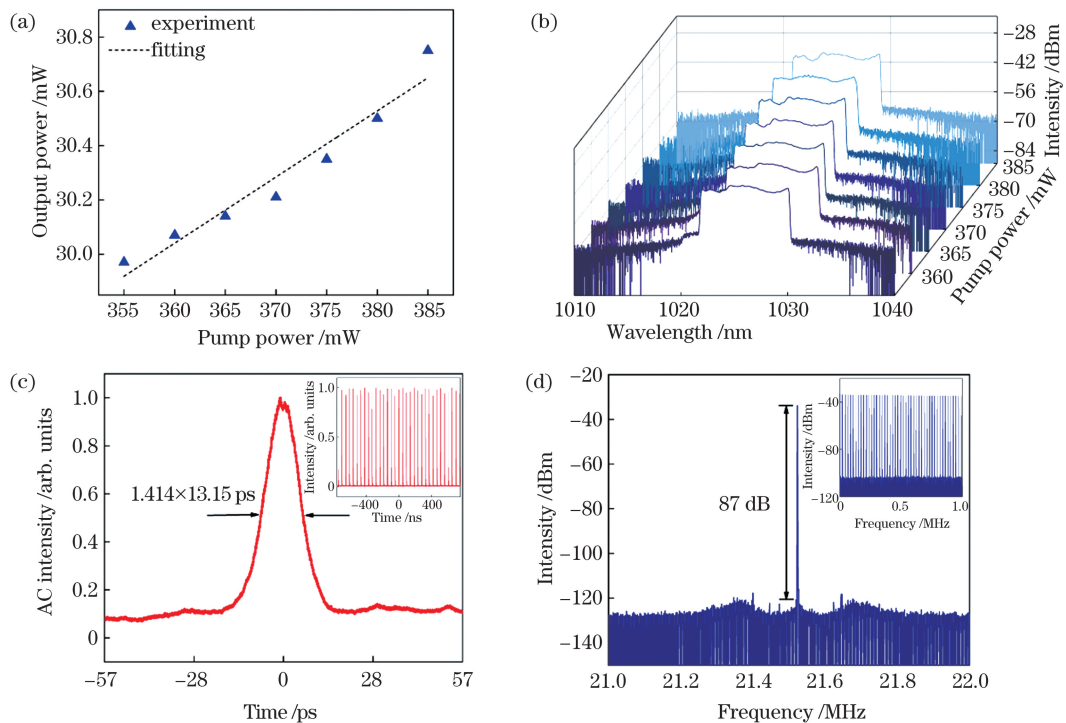


图 4 振荡级输出脉冲特性。(a) 输出功率随泵浦功率变化的曲线;(b) 不同泵浦功率下光谱演化图;(c) 泵浦功率为 375 mW 时输出自相关曲线;(d) 泵浦功率为 375 mW 时输出 RF 谱线
 Fig. 4 Output pulse characteristics of oscillator. (a) Output power varies with pump power; (b) spectral evolution under different pump powers; (c) AC trace when pump power is 375 mW; (d) RF spectrum when pump power is 375 mW

化的曲线,从图中可以看出,在锁模范围内输出功率随泵浦功率的增大而线性增加。图 4(b)为不同功率下的耗散孤子“猫耳型”光谱,光谱波长保持在 1021~1029 nm 附近,从图中可以看出,由于滤波效应的存在,光谱具有陡峭的边沿,随着泵浦功率的增加,光谱形状基本保持不变。为了优化锁模状态,将泵浦功率调至 375 mW,此时激光器输出功率为 30.14 mW,图 4(c)为该功率下激光器的输出脉冲自相关曲线和长程脉冲序列。可以看出,输出脉冲宽度为 13.15 ps,脉冲间隔为 46.4 ns,经计算可得脉冲能量为 1.4 nJ,峰值功率为 106.3 W。图 4(d)为输出脉冲的射频频谱图,激光器重复频率为 21.5 MHz,其信噪比为 87 dB,1 GHz 范围内 RF 谱

线轮廓整齐,可以看出该锁模状态具有较高的稳定性。

在实验过程中观察到了激光器从连续光状态到耗散孤子状态的建立过程,图 5(a)为泵浦功率 375 mW 时的实验测量图,图 5(b)为模拟仿真结果。从图 5(a)的实验结果可以看出,在脉冲建立之前,示波器显示为连续光状态,之后逐渐有小脉冲出现,并且峰值逐渐提高,直至脉冲峰值达到最高,随后经历一小段的下降后逐渐变得稳定,形成耗散孤子锁模。图 5(b)的模拟仿真图是图 2(a)的侧视图,从模拟结果可以看出,锁模的建立过程经历了脉冲峰值提高阶段、高峰值阶段和稳定锁模阶段,与实验结果基本吻合。

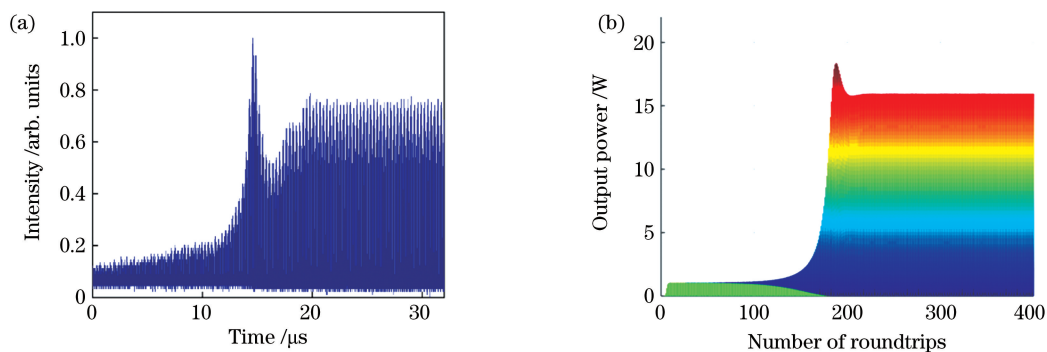


图 5 耗散孤子脉冲建立过程。(a) 实验结果;(b) 模拟仿真结果

Fig. 5 Establishment process of DS state. (a) Experimental results; (b) simulation results

振荡级产生的种子光通过可调滤波器可以产生不同中心波长的脉冲光,如图 6(a)所示,中心波长可调范围为 1022~1030 nm,透过滤波器的光谱面积随着波长的增加先增大后减小,可知此时振荡级输出的能量主要集中在中心波长 1025 nm 附近;而 1022 nm 和 1030 nm 的光谱具有明显的边沿陡峭形

状,证明其透过部分为耗散孤子光谱的两边沿部分。为了对 1024 nm 的激光进行放大研究,本文将可调滤波器中心波长调至 1024 nm,此时输出功率为 2.2 mW,脉冲能量为 0.1 nJ,脉冲序列如图 6(b)所示,可见锁模脉冲依旧保持稳定,但由于输出功率较低无法测量自相关曲线。

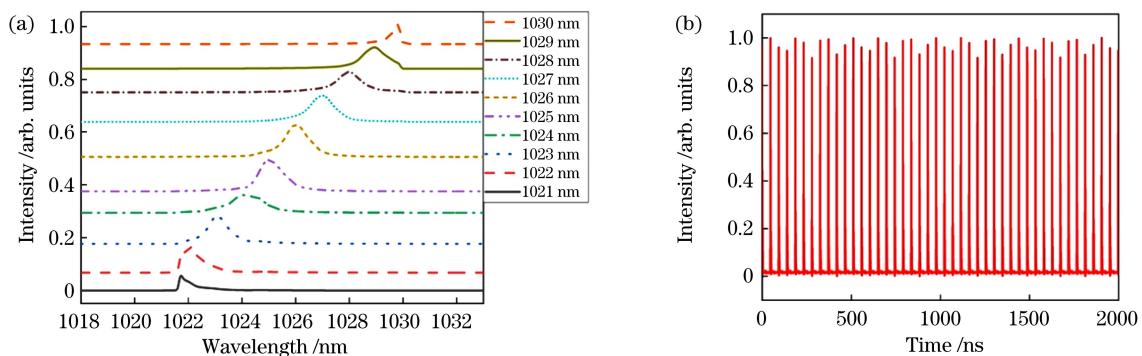


图 6 可调滤波后输出结果。(a)不同波长输出光谱;(b)1024 nm 处输出脉冲序列

Fig. 6 Output results after tunable filter. (a) Spectrum at different wavelengths; (b) output pulse sequence at 1024 nm

由于光谱滤波后,脉冲输出功率大幅降低,因此在可调滤波器之后增加了一级预放大装置。振荡级

泵浦源输出功率固定在 375 mW,可调滤波器中心波长调至 1024 nm,增加预放大级泵浦功率至

300 mW, 输出功率曲线如图 7(a) 所示, 光谱变化如图 7(b) 所示, 随着泵浦功率增加光谱峰值功率逐渐上升, 同时光谱宽度变宽, 在长波长方向产生新的光谱成分。长波长处的光谱成分主要是可调滤波器滤波效果有限导致的, 部分未被完全滤除的光谱成分被预放大级放大。当泵浦功率增加至 200 mW 以后, 光谱峰值部分会分裂出新的峰值, 这可能是较高的峰值功率引起的非线性效应导致的。因此为

了获得光谱能量更集中、峰值功率更高的脉冲, 将放大级泵浦功率设定在 200 mW, 此状态下预放大级输出功率为 42.02 mW。自相关曲线如图 7(c) 所示, 脉宽为 8.55 ps(相比于振荡级输出脉冲有所窄化, 这是滤波导致的), 脉冲能量为 1.95 nJ, 脉冲峰值功率为 228.1 W。图 7(d) 为 RF 谱线, 重复频率为 21.5 MHz, 信噪比为 82.4 dB, 且具有较好的长程射频稳定性。

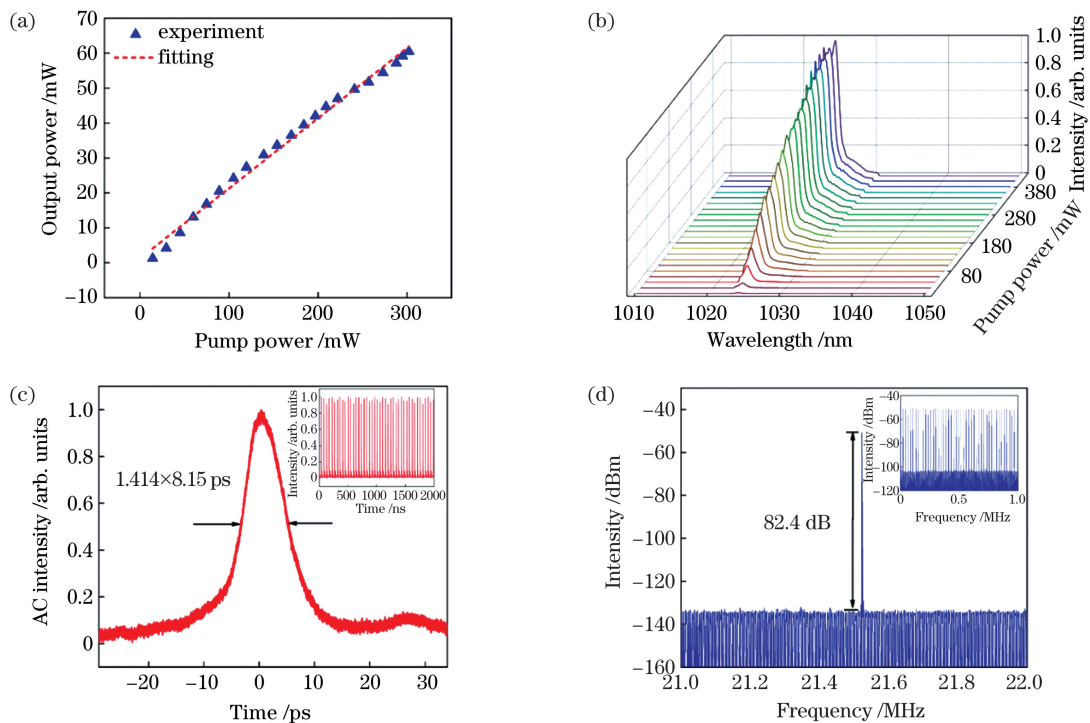


图 7 激光器预放大级输出脉冲特性。(a) 输出功率曲线; (b) 不同功率下输出光谱演化; (c) 脉冲自相关曲线; (d) RF 谱线
Fig. 7 Output pulse characteristics of laser pre-amplifier. (a) Output power curve; (b) output spectrum evolution under different pump powers; (c) pulse autocorrelation curve; (d) RF spectrum

为了获得更大的脉冲能量和峰值功率, 对脉冲进行了放大, 输出脉冲特性如图 8 所示。图 8(a) 为放大后输出功率随泵浦功率变化的曲线, 呈线性增加趋势。不同泵浦功率下的输出光谱如图 8(b) 所示, 在最大泵浦功率为 5 W 时, 输出平均功率为 1.1 W, 脉冲能量为 51 nJ, 可以看出, 随着泵浦功率的增加, 光谱强度逐渐上升, 脉冲能量主要集中在短波长部分, 光谱覆盖 1022 ~ 1030 nm 范围。光谱中仍然存在长波长部分, 这可能是可调滤波器的滤波效果与放大级增益导致的。对比之前的实验研究报道, 采用耗散孤子作为种子源的 MOPA 结构, 输出光谱通常达数十纳米甚至数百纳米^[16,25], 本文的放大器输出光谱宽度为 8 nm, 相对较窄, 进一步光谱压缩实验正在进行中。图 8(c) 为泵浦功率为 5 W 时的脉冲长程序列,

可以看出, 放大级输出锁模脉冲具有较好的稳定性。图 8(d) 为脉冲的 RF 频谱图, 其基频信噪比为 67.5 dB, 重复频率为 21.5 MHz, 插图 1 GHz 范围内长程 RF 谱线, 展现出了较好的稳定性。

5 结 论

本文理论上基于金斯伯格-朗道方程模拟了 NPR 锁模的全正色散掺 Yb 光纤激光器中耗散孤子脉冲的演化过程, 实验上获得了耗散孤子脉冲输出, 并且研究了锁模脉冲的建立过程, 将其与理论仿真结果相比, 结果基本吻合。将种子光脉冲通过可调滤波器, 获得了中心波长在 1020 ~ 1030 nm 处的一系列脉冲。选取中心波长为 1024 nm 的激光作为种子光, 经过预放大后获得脉冲宽度为 8.55 ps、

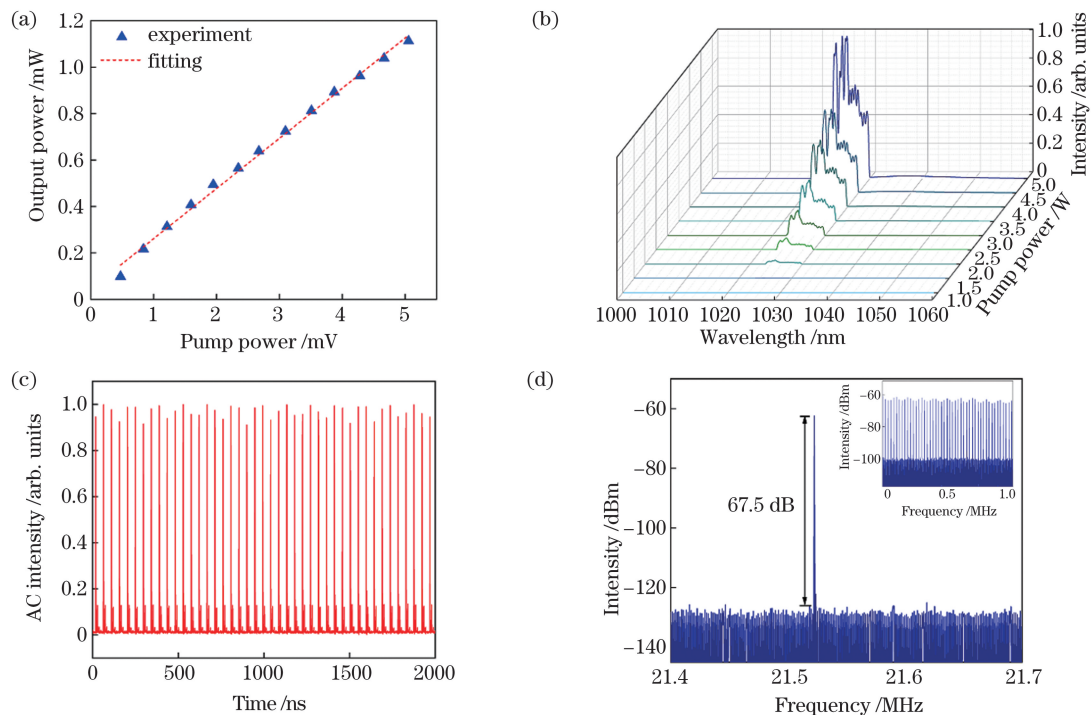


图 8 放大级输出脉冲特性。(a) 放大后输出功率随泵浦功率变化的曲线;(b) 不同功率下的输出光谱;(c) 泵浦功率为 5 W 时脉冲序列;(d) 泵浦功率为 5 W 时 RF 谱线

Fig. 8 Output pulse characteristics of main amplifier. (a) Output power curve change with pump power after amplification; (b) output spectrum under different pump powers; (c) pulse sequence when pump power is 5 W; (d) RF spectrum when pump power is 5 W

输出平均功率为 42.02 mW 的激光。再经过主放大级放大,当放大级泵浦功率为 5 W 时,获得输出平均功率为 1.1 W、脉冲能量为 51 nJ、中心波长为 1024 nm 的脉冲。光谱中仍然存在长波长部分,主要是由于可调滤波器的滤波效果有限,但相较于目前的实验研究报道,此放大级光谱输出宽度已经明显窄化,进一步光谱压缩实验正在进行中。此研究结果有助于人们深入理解 NPR 模光纤激光器中耗散孤子锁模动力学特性,同时此波段的脉冲激光有望应用于角分辨光电子能谱测量等领域。

参 考 文 献

- [1] Huang H, Yang L M, Liu J. Ultrashort pulsed fiber laser welding and sealing of transparent materials[J]. Applied Optics, 2012, 51(15): 2979-2986.
- [2] Joo C, Zhan C, Li Q, et al. Autoconfocal transmission microscopy based on two-photon-induced photocurrent of Si photodiodes[J]. Optics Letters, 2010, 35(1): 67-69.
- [3] Swann W C, Newbury N R. Frequency-resolved coherent LIDAR using a femtosecond fiber laser[J]. 2006 Conference on Lasers and Electro-Optics and 2006 Quantum Electronics and Laser Science Conference, 2006: 1-2.
- [4] Romero-Alvarez R, Pettus R, Wu Z, et al. Two-color fiber amplifier for short-pulse, mid-infrared generation[J]. Optics Letters, 2008, 33(10): 1065-1067.
- [5] Liang C, Lee K F, Levin T, et al. Ultra stable all-fiber telecom-band entangled photon-pair source for turnkey quantum communication applications[J]. Optics Express, 2006, 14(15): 6936-6941.
- [6] Guoyu H Y, Song Y R, Li K X, et al. Mode-locked ytterbium-doped fiber laser based on tungsten disulphide[J]. Laser Physics Letters, 2015, 12(12): 125102.
- [7] Zhang Y J, Liu J, Cai Y W, et al. Research on vibration performance of all-polarization-maintaining erbium-doped mode-locked fiber laser based on carbon nanotube[J]. Chinese Journal of Lasers, 2020, 47(9): 0901003.
张亚静, 刘杰, 蔡娅雯, 等. 碳纳米管锁模全保偏掺铒光纤激光器的振动性能的研究[J]. 中国激光, 2020, 47(9): 0901003.
- [8] Xu R Q, Tian J R, Song Y R. Noise-like pulses with a 14.5 fs spike generated in an Yb-doped fiber nonlinear amplifier[J]. Optics Letters, 2018, 43(8): 1910-1913.
- [9] Zhu X J, Geng J, Zhang G A, et al. Tunable double

- pulse dissipative solitons Yb-doped fiber laser based on Sagnac loop[J]. *Acta Optica Sinica*, 2019, 39(4): 0414002.
- 朱晓军, 耿健, 章国安, 等. 基于 Sagnac 环的可调谐双脉冲耗散孤子掺 Yb 光纤激光器[J]. *光学学报*, 2019, 39(4): 0414002.
- [10] Xu Z, Jia D F, Li Z H, et al. Generation of square pulses at both anomalous and normal dispersion regimes in passively mode-locked erbium-doped fiber laser[J]. *Chinese Journal of Lasers*, 2020, 47(12): 1201006.
- 徐震, 贾东方, 李梓豪, 等. 反常和正常色散区被动锁模掺铒光纤激光器的方波脉冲产生[J]. *中国激光*, 2020, 47(12): 1201006.
- [11] Matsas V J, Newson T P, Zervas M N. Self-starting passively mode-locked fibre ring laser exploiting nonlinear polarisation switching [J]. *Optics Communications*, 1992, 92(1/2/3): 61-66.
- [12] Tamura K, Ippen E P, Haus H A, et al. 77-fs pulse generation from a stretched-pulse mode-locked all-fiber ring laser[J]. *Optics Letters*, 1993, 18(13): 1080-1082.
- [13] Tamura K, Ippen E P, Haus H A. Pulse dynamics in stretched-pulse fiber lasers[J]. *Applied Physics Letters*, 1995, 67(2): 158-160.
- [14] Buckley J, Kuznetsova L, et al. Generation of 36-femtosecond pulses from a ytterbium fiber laser[J]. *Optics Express*, 2003, 11(26): 3550-3554.
- [15] Xiao X S, Hua Y. Supercontinuum generation based on all-normal-dispersion Yb-doped fiber laser mode-locked by nonlinear polarization rotation: influence of seed's output port [J]. *Optics Communications*, 2016, 377: 94-99.
- [16] Xu C X, Tian J R, Xu R Q, et al. Generation of noise-like pulses with a 920 fs pedestal in a nonlinear Yb-doped fiber amplifier[J]. *Optics Express*, 2019, 27(2): 1208-1216.
- [17] Wu X, Tang D Y, Zhang H, et al. Dissipative soliton resonance in an all-normal-dispersion erbium-doped fiber laser[J]. *Optics Express*, 2009, 17(7): 5580-5584.
- [18] Jiang G B, Chen Y, Wang L L, et al. Wavelength tunable noise-like pulse generation from an erbium-doped fiber laser [J]. *Journal of Optics*, 2019, 21(1): 015502.
- [19] Du Y Q, Xu Z W, Shu X W. Spatio-spectral dynamics of the pulsating dissipative solitons in a normal-dispersion fiber laser [J]. *Optics Letters*, 2018, 43(15): 3602-3605.
- [20] Zawischa I, Plamann K, Fallnich C, et al. All-solid-state neodymium-based single-frequency master-oscillator fiber power-amplifier system emitting 5.5 W of radiation at 1064 nm[J]. *Optics Letters*, 1999, 24(7): 469-471.
- [21] Ye C G, Gong M L, Yan P, et al. Linearly-polarized single-transverse-mode high-energy multi-ten nanosecond fiber amplifier with 50 W average power [J]. *Optics Express*, 2006, 14(17): 7604-7609.
- [22] Lin H Q, Guo C Y, Ruan S C, et al. 20-W wavelength-tunable picosecond Yb-doped fiber MOPA source seeded by an NPR mode-locked fiber laser[J]. *IEEE Photonics Journal*, 2014, 6(5): 1-6.
- [23] He Y, Vishik I, Yi M, et al. High resolution angle resolved photoemission with tabletop 11 eV laser [EB/OL]. (2015-09-04) [2020-11-02]. <https://arxiv.org/abs/1509.01311>.
- [24] Loiko P A, Serres J M, Mateos X, et al. Passive Q-switching of Yb bulk lasers by a graphene saturable absorber[J]. *Applied Physics B*, 2016, 122(4): 1-8.
- [25] Guo J Y, Xu R Q, Fan L Y, et al. Mechanism of broadband spectrum generation based on nonlinear ytterbium-doped fiber amplifier[J]. *Chinese Journal of Lasers*, 2019, 46(9): 0901009.
- 郭瑾颐, 徐润亲, 范路遥, 等. 非线性掺铒光纤放大器产生宽光谱机理[J]. *中国激光*, 2019, 46(9): 0901009.

Generation and Amplification of a 1024 nm Mode-Locked Laser Based on a Tunable Fiber Filter

Cui Youshuo, Zhang Lulu, Yin Jie, Dong Zikai, Hua Lingling,
Tian Jinrong, Song Yanrong*

Faculty of Science, Beijing University of Technology, Beijing 100124, China

Abstract

Objective Angular-resolved photoemission spectroscopy (ARPES) is a powerful and unique technique used to study the electron structure in condensed matter. It can directly obtain the energy band structure and electron self-energy

by momentum resolution. A 1024 nm laser can be used as an ARPES source after multiple frequency doubling, such as the measurement of charge density wave gaps of telluride of rare earth elements. The main emission peak of Yb^{3+} ions is near 1064 nm; hence, the emission of the 1024 nm pulse laser is relatively difficult, requiring the fine control of the filter parameters. Thus far, reports on the 1024 nm laser are mainly concentrated on solid-state lasers. A fiber laser has the advantages of compact structure, low cost, and good stability. The low output power of the fiber laser can be made up by the amplifier, which has a good application value.

Methods In this study, pulse evolution in a fiber laser was numerically simulated by the system of the coupled Ginzburg-Landau equation and solved using the split-step Fourier method. The laser passed through each device in turn in the cavity and repeatedly circulated. The pulse formation and evolution were simulated. Experimentally, the seed source was an all-normal dispersion Yb-doped fiber laser mode-locked by nonlinear polarization rotation (NPR). The oscillator consisted of a 976 nm pump, a 980/1030 nm wavelength division multiplexer (WDM), a piece of 54 cm Yb-doped fiber (YDF), an isolator polarization-independent isolator, an output coupler, and an NPR saturable absorber. A master oscillator power amplifier system based on a tunable fiber filter was built to realize the 1024 nm output laser. The seed pulse was filtered by a tunable filter. Subsequently, preamplification and amplification experiments were conducted. The preamplifier contained a pump, a WDM, a piece of YDF, and an isolator, while the amplifier comprised a pump, a WDM, and a piece of YDF. The laser was output by a collimating isolator. The output laser parameters were measured by a 12.5 GHz photoelectric detector, a 6 GHz oscilloscope, a spectrograph (Yokogawa, AQ6370C), an autocorrelator (FR-103XL), and a frequency spectrograph (Agilent, E4447A). The seed laser formation was the NPR mechanism realized by the artificial saturable absorber formed by the wave plate, band pass filter, and polarization beam splitter. The NPR belongs to the fast saturation absorber mode locking mechanism; thus, it was more conducive for the ultrashort pulse generation.

Results and Discussions The dissipative soliton pulses can be generated when the simulated model parameters are appropriate (Fig. 2). The pulses gradually formed with the accumulation of the intracavity energy. Figures 2(b) and (c) depict the evolution of the spectral and pulse shapes at different locations in the cavity. The output pulse of the oscillator was a dissipative soliton with a steep edge spectrum. The established process of the mode-locked pulse was studied herein. The pulse establishment process included the peak power improvement, high peak power, and stable mode-locked stages. The experimental results were consistent with the theoretical simulation results. The seed laser generated by the oscillator can generate a pulse laser with different central wavelengths through the tunable filter (Fig. 6(a)). The tunable range of the central wavelength was 1022–1030 nm. We set the central wavelength of the tunable filter to 1024 nm. The pulse output power was greatly reduced because of the spectral filtering; hence, a preamplifier was added after the tunable filter. To obtain pulses with more concentrated spectral energy and higher peak power, the pump power of the amplifier was set to 200 mW, and the output power of the preamplifier was set to 42.02 mW. Figure 8 shows the output pulse characteristics of the main amplifier. When the pump power of the amplifier was 5 W, the stable output mode-locked laser was obtained with a central wavelength of 1024 nm, an average power of 1.1 W, a pulse energy of 51 nJ, a repetition frequency of 21.5 MHz, and a signal-to-noise ratio of 67.5 dB.

Conclusions This study theoretically simulated the evolution process of the dissipative soliton pulse in the NPR mode-locked Yb-doped fiber laser based on the Ginzburg-Landau equation. We experimentally obtained the dissipative soliton pulses and studied the establishment process of the mode-locked pulses. The results were basically consistent compared with the theoretical simulation results. A series of pulses with 1020–1030 nm central wavelength were obtained by passing the seed laser pulse through a tunable filter. The laser with a 1024 nm central wavelength was selected as the seed laser for amplification. The laser with 8.55 ps pulse width and 42.02 mW average output power was obtained after the preamplifier. After the main amplifier, when the pump power of the amplifier was 5 W, the output average power was 1.1 W, the pulse energy was 51 nJ, and the central wavelength was 1024 nm. A useless wavelength was found in the spectrum, which was mainly caused by the limited filtering effect of the tunable filter. However, compared with the current experimental research reports, the spectral output width of this amplifier is significantly narrowed, and further experiments on spectral compression are under way. The results are helpful in understanding the dynamic characteristics of dissipative soliton mode locking in the NPR mode-locked fiber laser. Furthermore, the pulse laser at this wave band is expected to be applied in ARPES measurement.

Key words lasers; fiber laser; mode-locked lasers; laser amplifiers; nonlinear polarization rotation; dissipative soliton

OCIS codes 140.3510; 140.4050; 140.3280